

An Acoustic Communication Model in Plants

Fatih Merdan, Ozgur B. Akan, Fellow, IEEE

Abstract—Molecular communication (MC) studies biological signals that are found in nature. Most MC literature focuses on particle properties, even though many natural phenomena exhibit wave-like behavior. One such signal is sound waves. Understanding how sound waves are used in nature can help us better utilize this signal in our interactions with our environment. To take a step in this direction, in this paper, we examine how plants process incoming sound waves and take informed actions. Indeed, plants respond to sound, yet no quantitative communication-theoretic model currently explains this behavior. This study develops the first end-to-end acoustic communication framework for plants. The model is formed following the biological steps of the incoming signal, and a mathematical description is constructed at each step following basic biological models. The resulting end-to-end communication-theoretic model is analyzed using MATLAB. Simulations show that a 200 Hz, 20 μPa stimulus elevates cytosolic Ca^{2+} from 150 nM to 230 ± 10 nM within 50 seconds which can cause root bending in plants in the long run. This work establishes quantitative phytoacoustics, enabling bio-inspired acoustic connections for precision agriculture and plant signaling research.

Index Terms—Communication systems, mathematical models, biological processes, plant communication, acoustic waves.

I. Introduction

PLANTS are constantly sensing their environments to make the best use of their available resources [1]. To achieve this, they must gather all kinds of information they can from different stimuli like light, temperature, moisture, stiffness of the soil, pH, touch, and sound waves which is the focus of this article. Phytoacoustics is the term coined for the study of how plants perceive, produce, and respond to sound waves. Even though the study of sound waves in plant kingdom can be traced back almost to 60 years ago [2], this topic is gaining more attention these days as the experimental studies conducted yield promising results [3], [4], [5], [6], [7]. However, several key questions remain open—for example, how plants sense sound waves without a dedicated hearing organ, and what internal decision processes govern their reactions to acoustic stimuli. Gaining deeper insights into these mechanisms is essential for integrating plant sensory behavior into Internet of Everything (IoE) based monitoring systems and advancing next-generation precision agriculture technologies [8], [9].

The authors are with the Center for neXt-generation Communications (CXC), Department of Electrical and Electronics Engineering, Koç University, Istanbul 34450, Türkiye (e-mail: {fmerdan25, akan}@ku.edu.tr).

Ozgur B. Akan is also with the Internet of Everything (IoE) Group, Electrical Engineering Division, Department of Engineering, University of Cambridge, Cambridge, CB3 0FA, UK (e-mail: oba21@cam.ac.uk).

The objective of this paper is to establish the first communication theoretical model for phytoacoustics in the literature. To the best of our knowledge, there is no communication theoretical approach explaining sound wave transmission and sensing in plants. In this paper, only the sensing of sound stimulus by plants is considered since even though there have been observed some patterns in sounds emitted by plants under stress [10], it is still not clear if plants can produce purposeful sound waves. However, it is now well established that plants sense and respond to sound waves [11], [12], [4]. Most of the research conducted on plants use the model plant *Arabidopsis Thaliana* because it has a short life cycle and easy to experiment on. Furthermore, it is the first plant whose genome is identified, and many mutation lines are available [13], [14]. This paper presents a communication theoretical model that focuses on the roots of the model plant *Arabidopsis Thaliana* under the sound waves created by water flow through the soil. The main structure of the proposed framework is shown in Fig. 1.

The rest of this paper is organized as follows. In Section II, the acoustic pathway in plants is discussed. In Section III, sound generation and transmission are explained. Sound perception by plants is explained in Section IV. In Section V, the mathematical framework of sound perception by plants is described. In Section VI, the simulation results are given and discussed. In Section VII, communication-theoretic analysis is conducted. The paper is finalized with the concluding remarks in Section VIII.

II. Acoustic Pathway in Plants

A sound wave is basically an oscillation of pressure levels. In essence, it can be considered as a mechanical stimuli. Plants sense mechanical stimuli, like touch and wind, through mechanosensing receptors on the plasma membranes of their cells. Mechanoperception mostly occurs by an increase in the cytosolic Ca^{2+} levels, since these mechanosensing receptors trigger a calcium flux through the cytosol. After sound stimuli, a similar Ca^{2+} behaviour also occurs in plants [16]. Therefore, we assumed that hearing in plants is facilitated by mechanically sensible Ca^{2+} channels.

Calcium channels are membrane proteins that regulate the flow of Ca^{2+} ions across cellular membranes, enabling signaling and physiological responses in cells. Ca^{2+} channels can be divided into two; voltage-dependent Ca^{2+} permeable channels (VDCCs) and voltage independent Ca^{2+} permeable channels (VICCs). VDCCs are divided into two groups: depolarization activated Ca^{2+} permeable channels (DACCs) and hyperpolarization activated Ca^{2+}

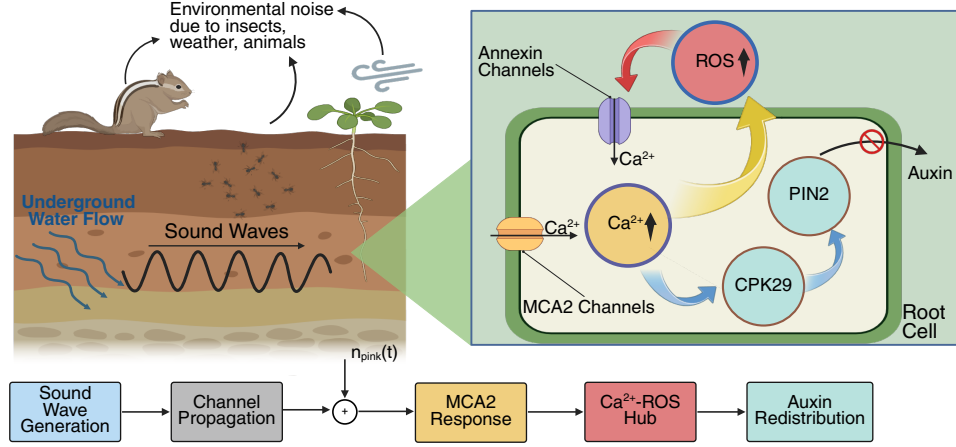


Fig. 1. The proposed end-to-end communication-theoretic framework for phytoacoustics. Sound waves activate MCA2 channels, leading to calcium influx with Ca^{2+} -ROS Hub activity, triggering CPK29 signaling, and modulation of PIN2-mediated polar auxin transport [15].

permeable channels (HACCs) [17], [18], [19]. Mechanoreceptors are considered in the VICCs group. ‘Mechanosensitive channels of small (MscS) conductance’-like channels, ‘mid1-complementing activity’ channels (MCAs), Piezo channels, and hyperosmolality-induced Ca^{2+} channels (OSCA) are the gene families that encode these channels [20]. Today, it is still not exactly clear which of these channels contribute to the perception of sound in plants and to what extent. However, most of them have an established place in plant metabolism. To determine a possible channel, we inspect the directional growth of a plant in response to a mechanical stimulus. Such mechanisms are studied under the term thigmotropism. It is found that MCA channels are important in this context [21], [22], [23], [24]. In fact, there are two types of MCA channels: MCA1 and MCA2 who share 72.7% amino acid sequence identity and several common structural features. MCA1 senses soil hardness and influences root bending to avoid hard soil to facilitate thigmotropism. MCA2 is also important for thigmotropism; however, its exact role relative to MCA1 in plant metabolism remains unclear. Therefore, we propose that MCA2 channels are responsible for sound perception in plant roots to fill this gap and assume it to be the main sensory unit for sound waves in this paper.

The main growth hormone in plants, which is effective in gravitropism and thigmotropism, is auxin [25], [26], [27]. Conversely, abicidic acid is primarily responsible for mediating the response to moisture stimuli [28], [29]. Considering sound waves as mechanical stimuli, the main hormone of interest in this paper is auxin.

The block diagram of the communication system is given in Fig. 1. Flow of water creates a sound wave which stands for the transmitter of the communication system. Then, this sound wave travels underground and reaches the root cells of the plant where it triggers MCA2 channels, which leads to a Ca^{2+} influx. Ca^{2+} influx increases the apoplastic reactive oxygen species (ROS) concentrations of the root cells. Especially high apoplastic H_2O_2 concentrations activates another type

of Ca^{2+} channel which increases cytosolic Ca^{2+} levels more. This positive feedback mechanism is referred to as the Ca^{2+} - ROS Hub, which eventually results in the redistribution of auxin in root cells.

III. Sound Generation and Transmission

Propagation of sound waves under porous media, e.g., soil follows Biot’s Theory [30], [31]. Considering soil as a communication channel, Kelvin–Voigt Model, which takes sound attenuation into account as well as both the viscous and elastic properties of the soil, has been used in this paper [32], [33]. Therefore, underground sound waves can be expressed as a function of time and space as

$$s(x, t) = A_s e^{k_2 x} e^{i(\omega t - k_1 x)}, \quad (1)$$

with,

$$k_1^2 = \frac{\rho \omega^2}{2G(1 + 4\zeta^2)} \left(\sqrt{1 + 4\zeta^2} + 1 \right), \quad (2)$$

$$k_2^2 = \frac{\rho \omega^2}{2G(1 + 4\zeta^2)} \left(\sqrt{1 + 4\zeta^2} - 1 \right), \quad (3)$$

$$\zeta = \frac{\eta \omega}{2G}, \quad (4)$$

where t is time, x is position, ζ is the damping ratio, $\omega = 2\pi f$ is the angular frequency, G is shear modulus (MPa), η is the viscosity of the material (Pas) and ρ is bulk density (gm/cm^3). Clay soil texture is assumed to be used and external sources are utilized for related parameters.

The frequency 200 Hz is associated with water flow, and plant roots are observed to follow the sound waves with this frequency [34], [16], [35]. Therefore, this frequency is used to model sound waves created by water flow. However, in nature, it is not possible for only sound waves with a frequency of 200 Hz to be created during water flow. Changes in the flow rate, interactions with obstacles, and turbulence effects may cause different frequencies to

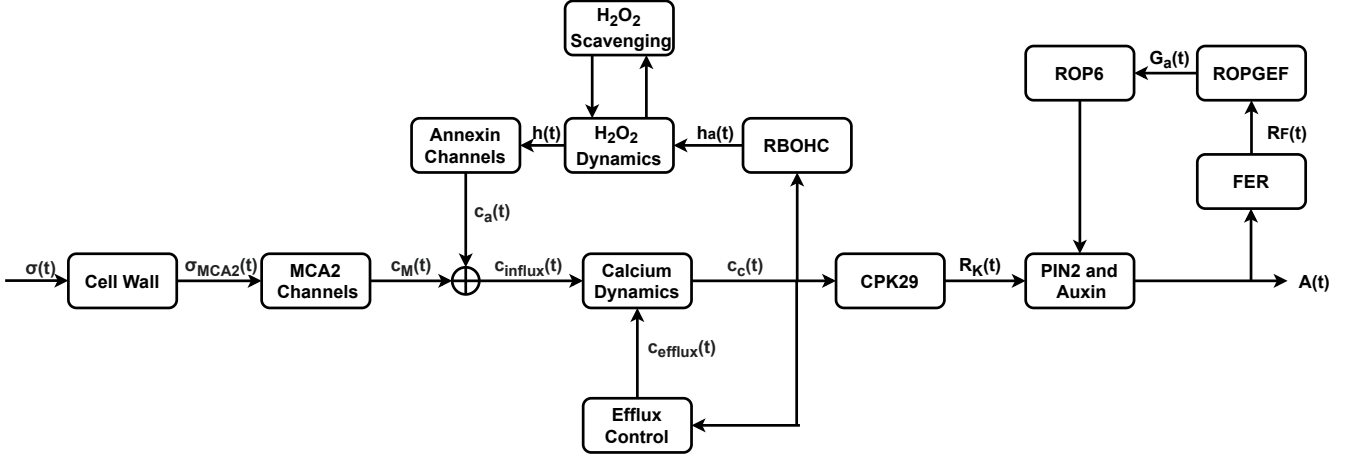


Fig. 2. Block diagram showing the proposed model for the sound perception by plants.

occur as the water flows. To account for this effect, the transmitted sound wave is expressed as

$$s(x, t) = \sum_{n=1}^{N_1} A_s e^{k_2 x} e^{i(\omega_n t - k_1 x)}, \quad (5)$$

where different frequencies can be created at the same time and f_n in $\omega_n = 2\pi f_n$ is treated as a Gaussian random variable with mean 200 *Hz* and standard deviation of 60 *Hz* which is decided by considering the spectrogram of the recorded sound of water flow through a pipe [35]. Moreover, a random phase between 0 and 2π is added for each sound wave. The amplitude A_s is also taken as a Gaussian random variable with mean 20 μPa and a standard deviation of 1 μPa .

Since Kelvin-Voigt Model already describes the attenuation and phase changes of the propagating sound waves, for expressing the channel response, one should only insert the distance value to (5). Therefore, the channel impulse response is modelled as

$$h_c(x) = \delta(x - x_m), \quad (6)$$

where x_m is used to describe the distance between the water and the root cells. Moreover, there could be environmental sounds created by insects, weather, animals, or humans. To account for this effect, pink noise is added to the output of the channel. Pink noise has a power spectrum that decays with $1/f$ and this means only low frequency sounds will have a considerable effect. This correlates with sound waves propagating through the soil, as it can be observed in (1) and (3); the higher the frequency, the higher the decay.

IV. Sound Perception by Plants

The structures called trichomes are the first to sense the sound wave oscillations, and they work as antennae for sound stimulus [36], [37], [38]. However, they do not exist in the root cells; therefore, when a sound wave reaches the root cells of the plant, the first structure it interacts

with is the cell wall. In [39], a mathematical model is presented that explains how pressure applied to the cell wall affects the small protein-like structures such as MCA2 channels on the cell membrane. In this paper, this model is utilized. MCA2 channels have been studied previously and it is found that four of these proteins can form a channel structure (tetramer structure) [40], [41]. Previous studies provide information about opening probabilities and current flow through MCA2 channel, which enables one to find the increase in the Ca^{2+} concentration in the cytosol.

Increasing levels of Ca^{2+} in cytosol triggers NADPH oxidase RBOHC (Respiratory burst oxidase homolog protein C) to activate. Ca^{2+} binds to the EF-hand domains of the RBOHC which makes the protein undergo a conformational change, which, in the end, activates it [42], [18]. NADPH oxidases are responsible for the production of extracellular ROS (reactive oxygen species) which is another secondary messenger in plant biology. Especially, apoplastic Hydrogen Peroxide (H_2O_2) levels increase after the activation of RBOHC. Apoplastic H_2O_2 binds to annexin channels, which are binding-activated Ca^{2+} channels on the plasma membrane, and this triggers more Ca^{2+} to flow into cytosol [18]. This positive feedback mechanism makes sure that there is a high Ca^{2+} concentration inside the cell [43], [44].

High cytosolic Ca^{2+} also activates the CPK29 (calcium-dependent protein kinase 29) by a similar EF-hand Ca^{2+} binding mechanism. CPK29 is a calcium-dependent protein kinase that functions in the phosphorylation of PIN2 proteins [45]. PIN family of proteins play a critical role in the regulation of auxin transport in plants.

Auxin levels of the cells of the *Arabidopsis Thaliana* are regulated by mainly two types of transporters. The entry of auxin into cells is primarily mediated by AUX1 transporters. Since most cells have symmetric distributions of AUX1, polar auxin transport is achieved by regulation of PIN carriers, which are the main efflux transporters of auxin [25]. Therefore, the regulation of PIN2 localization may result in polar auxin transport, which eventually

causes one side of the root to grow longer, leading to bending.

There are two main mechanisms in the regulation of PIN proteins: Endocytosis refers to the removal of PINs from the plasma membrane, temporarily reducing auxin transport out of the cell in a specific direction. Recycling of PINs refers to the process by which PIN proteins are continuously cycled between the plasma membrane and internal cellular compartments. It is observed that CPK29 directly binds to PIN2 and an energy transfer occurs between the two [45]. However, it is not established whether this results in the endocytosis of PIN2 proteins, or recycling of PIN2 proteins back to the plasma membrane. In this paper, we assume that CPK29 activity results in the endocytosis of PIN2 proteins. Because, this way, the side of the root that is closer to the water flow will not have much auxin in its root tips, and the other side will grow longer. This results in the bending of the root towards the water.

There is another pathway that influences PIN2 localization, which is triggered by apoplastic auxin [46]. Apoplastic auxin triggers the receptor like-kinase FERONIA to be activated by binding to it. Activated FERONIA directly engages with Rop-guanine nucleotide exchange factors (RopGEFs), which promote the exchange of GDP for GTP, transitioning RAC/ROPs from their inactive GDP-bound state to their active GTP-bound state [47]. In this paper, ROP6 is considered because it is found that it causes the inhibition of PIN2 internalization which means it blocks endocytosis of PIN2 [48], [49].

V. Mathematical Modelling of Sound Perception by Plants

The proposed model for sound perception by plants is given in Fig. 2. As described in [39], using the stress on the cell walls, one can find the force applied on MCA2 proteins, $F(t)$. It can be expressed as

$$F(t) = \frac{\mu_s}{\mu_w} \left(\frac{\tau_w}{\tau_s} \Delta_{\tau_s} \tilde{\sigma}(t) + \langle \tilde{\sigma}(t) \rangle_{\tau_s} \right), \quad (7)$$

with

$$\langle \tilde{\sigma}(t) \rangle_{\tau_s} = \int_{-\infty}^0 \frac{d\tau}{\tau_s} e^{\frac{\tau}{\tau_s}} \tilde{\sigma}(t + \tau), \quad (8)$$

$$\Delta_{\tau_s} \tilde{\sigma}(t) = \tilde{\sigma}(t) - \langle \tilde{\sigma}(t) \rangle_{\tau_s}, \quad (9)$$

$$\tilde{\sigma}(t) = \sigma - Y, \quad (10)$$

where the cell wall is modeled as a viscoelastoplastic material consisting of a spring of elastic modulus K_w in series with a dashpot of viscosity μ_w , arranged in parallel with a frictional block that has a yield stress Y , which is the stress beyond which the wall begins to exhibit viscous behavior. $\tau_w = \mu_w/K_w$ is the relaxation time. The sensor (MCA2) is assumed to be embedded in a viscoelastic medium, arranged in parallel with the wall, and

characterized by an elastic modulus K_s , and a viscous coefficient μ_s . The relaxation time, $\tau_s = \mu_s/K_s$, defines the point at which the medium begins to display viscous behavior. $\langle \tilde{\sigma}(t) \rangle_{\tau_s}$ is the slow tend of stress $\tilde{\sigma}(t)$.

To find the pressure applied on one MCA2 channel $\sigma_{MCA2}(t)$, the resulting force is divided by the surface area of the MCA2 channels, A_M which is calculated by assuming MCA2s as cylinders, taking into account the tetramer structure of the channels and the size values from [40].

A. MCA2 Channels

MCA2 block in Fig. 2 can be further expanded as shown in Fig. 3. MCA2 channels have activation, inactivation, and deactivation phases. This mechanism can be supported by the study in [41], where current curves have almost periodic spikes and zero values between the spikes indicate the channel being closed for some time. This phenomenon results in higher-frequency stimuli being eliminated. Therefore, the first block in the MCA2 block diagram is a low-pass filter.

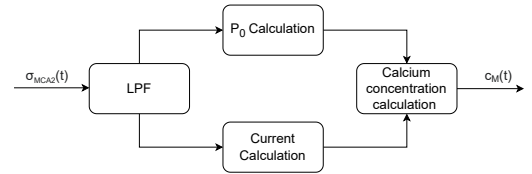


Fig. 3. Block diagram modelling MCA2 channels.

Using the data provided in [41], the probability of the MCA2 channel being in the open state is observed to be exponentially dependent on voltage. Such relationships can be modeled using the Boltzmann distribution, and a reasonable curve is fit to the measurement data shared in [41]. The resulting function describing the voltage dependence of the probability of open state, P_0 , is given as

$$P_0(V) = \frac{1}{1 + e^{\frac{V_h - V}{k_V}}}, \quad (11)$$

where V_h corresponds to the voltage at which the probability of the MCA2 channel being in the open state is 50%. Similarly, the pressure dependence of this probability is found and given as

$$P_0(\sigma) = \frac{1}{1 + e^{\frac{\sigma_h - \sigma}{k_\sigma}}}, \quad (12)$$

where σ_h corresponds to the stress level at which the probability of the MCA2 channel being in the open state is 50%. Using the fact that pressure data is obtained for 150 mV, the total open state probability function is described as

$$P_0^{MCA}(V, \sigma) = l \times \frac{1}{1 + e^{\frac{V_h - V}{k_V}}} \times \frac{1}{1 + e^{\frac{\sigma_h - \sigma}{k_\sigma}}}. \quad (13)$$

Ca^{2+} will flow into the cytosol when MCA2 channels become open because of both the concentration gradients and electric fields. Therefore, the current that passes through the MCA2 channels can be expressed using the Nernst-Planck electrodiffusion equation [50]. Here, the derivatives are simplified into changes in the electric potential and concentration difference of Ca^{2+} ions, i.e.,

$$I_M = -z_{Ca} F D_{Ca} \left(\frac{\Delta c}{\Delta x_d} + \frac{F z_{Ca} c_c}{RT} \frac{\Delta E}{\Delta x_d} \right) \times A_C, \quad (14)$$

with diffusion coefficient D_{Ca} is modified so that it depends on the applied pressure, i.e.,

$$D_{Ca} = \frac{RT}{F} u_{Ca} (1 + k_d \sigma_f), \quad (15)$$

where $z_{Ca} = 2$ is the valence of ion Ca^{2+} , R is the universal gas constant, T is the absolute temperature, F is the Faraday's constant, u_{Ca} is the mobility of ions, σ_f is the filtered pressure on one MCA2 channel, Δc is the concentration gradient and ΔE describes the potential of the cell membrane, Δx_d is the thickness of the cell membrane and A_C is the surface area where Ca^{2+} ions can flow through. In [50], $D_{Ca} = 0.79 * 10^{-5} cm^2/s$ is provided without the dependence of σ_f . Normally, Ca^{2+} concentration in the extracellular space is about 1-10 mM, where inside the cell it is between 100-200 nM in resting conditions [51], [52]. Because of this significant difference, Δc can be considered constant throughout the process. Even though ΔE may change and there may occur an electrical signal on the plasma membrane (action potentials or variation potentials), modeling it requires considering all kinds of ionic movements like K^+ , Mg^{2+} [53]. In this, for the sake of simplicity, ΔE is also considered as a constant.

Having found the probability of the MCA2 channel being in the open state, and the current it creates, the concentration of the Ca^{2+} ions that are added to the cytosol can be found using the total probability theorem as

$$c_M(t) = \frac{I_M t}{z_{Ca} V} \times P_0 \times n_C, \quad (16)$$

where V is the cytosolic volume of the root cells and n_C is the number of MCA2 channels.

B. Calcium Dynamics

Steady state cytosolic calcium concentration is taken as $c_{ss} = 150$ nM in root cells. The main calcium influx sources are the MCA2 and annexin channels. These channels are separately studied in the model. There are many mechanisms that decrease the cytosolic calcium concentration. For example, EF-hands of many calcium protein kinases or other proteins accumulate some Ca^{2+} , excess calcium can diffuse to neighboring cells through the structures called plasmodesmata [54], [55]. Moreover, all organelles can store some amount of calcium; however, the vacuole and endoplasmic reticulum (ER) serve as

the largest calcium storage sites [56]. In this paper, we assumed the following simplified efflux control block

$$c_{efflux}(t) = \begin{cases} Q, & \text{if } c_c(t) \geq 200 \\ k_{eff2}(c_c(t) - 155), & \text{if } 165 \leq c_c(t) < 200 \end{cases}, \quad (17)$$

where $Q = \max(k_{eff1}(c_c(t) - 195), k_{eff2}(c_c(t) - 155))$ and c_c is the cytosolic Ca^{2+} concentration in nM, so that under high difference from the steady state value, the decrease of Ca^{2+} will be higher as observed in nature. Calcium Dynamics block basically applies the following starting from the time instance zero and where t' represents the previous time instance

$$c_c(t) = c_c(t') + c_{influx}(t) - c_{efflux}(t). \quad (18)$$

C. H_2O_2 Dynamics

Cytoplasmic calcium binds to the EF-hands of the RBOHC and activates it. Activation of a larger protein by smaller structures can be modeled using the Hill equation. Considering RBOHC has 2 EF-hand structures, and two Ca^{2+} can bind to it simultaneously, the Hill equation is of the form

$$R_C = \frac{c_c^2}{k_C + c_c^2}, \quad (19)$$

where R_C represents the fraction of Ca^{2+} bound (activated) RBOHCs. The total RBOHC concentration in Arabidopsis Thaliana is calculated using (20) established in [57] where related ppm values are obtained from online databases.

$$C_{total} = \frac{k_{ppm} AB}{N_A}, \quad (20)$$

where C_{total} is the total concentration, N_A is the Avagadro Constant, and AB is the abundance value where 1ppm means $AB = 10^{-6}$. This idea is also used to find the total concentrations of CPK29, FERONIA, PIN2, ROPGEF4, and ROP6 proteins. These values are provided in Table II. Using the total RBOHC concentration and R_C , one can find the activated RBOHC concentration, C_{ac} by multiplying the two.

In this paper, the Michaelis-Menten equation which is a general relation describing how enzymes catalyze reactions is used to model the H_2O_2 generation by RBOHC [58]

$$v_H = \frac{v_{Hm} C_{ac}(t)}{m_H + C_{ac}(t)}, \quad (21)$$

where v_H is the reaction rate (velocity) of the process, v_{Hm} is the maximum reaction velocity and m_H is the Michaelis constant for this reaction. Integrating v_H with time gives the concentration of H_2O_2 in apoplast created by RBOHC, h_a .

H_2O_2 scavenging refers to the breakdown of hydrogen peroxide by apoplastic catalases. This enzymatic reaction can also be modeled using the Michaelis-Menten equation as follows

$$v_s = \frac{v_{sm}h(t)}{m_s + h(t)}, \quad (22)$$

where v_s is the reaction rate of the scavenging, v_{sm} is the maximum reaction velocity, $h(t)$ is the apoplasmic H_2O_2 concentration, m_s is the Michaelis constant for this reaction. Integrating v_s with time gives the broken down H_2O_2 concentration, h_s .

Inside the H_2O_2 Dynamics block the following operation is performed and apoplasmic H_2O_2 concentration $h(t)$ is given as the output

$$h(t) = h(t') + h_a(t) - h_s(t) \quad (23)$$

where t' represents the previous time instance.

D. Annexin Channels

Annexin channels are ligand-gated channels activated by apoplasmic H_2O_2 . Such channels can be modeled by the following relation [52]

$$I_a = G_a \frac{[h(t)]^z}{[h(t)]^z + k_a^z} (E_c - \Delta E), \quad (24)$$

where G_a is the channel conductance of the annexin channel, ΔE is the cell membrane voltage, k_a^z is the ligand concentration producing a half-maximal response, and z is the Hill coefficient, which theoretically represents the number of binding sites. The Nernst equation, i.e.,

$$E_c = \frac{RT}{zCaF} \ln \frac{c_{ap}}{c_c(t)}, \quad (25)$$

can be used to determine the membrane voltage, E_c , known as the equilibrium or reversal potential, which would keep the apoplasmic ($c_{ap}(t)$) and cytosolic ($c_c(t)$) Ca^{2+} concentrations in a steady state [52].

Using the current relation of annexin channels, one can calculate the concentration of the Ca^{2+} ions that are added to the cytosol by

$$c_a(t) = \frac{I_a t}{zCaV} \times n_a, \quad (26)$$

where V is the cytosolic volume of the root cells and n_a is the number of annexin channels.

E. CPK29

Similar to Ca^{2+} activation of RBOHC, Ca^{2+} activation of CPK29 can be modeled using Hill equation taking into account that CPK29 has 4 EF-hand structures

$$R_K = \frac{c_c^4}{k_K + c_c^4}, \quad (27)$$

where R_K represents the fraction of Ca^{2+} bound (activated) CPK29s. Multiplying this result with the total CPK29 concentration given in Table II, one can find the activated CPK29 concentration, K_{ac} . Then, CPK29 phosphorylates PIN2, a process that can be described using Michaelis-Menten kinetics. However, in this case, the

Goldbeter-Koshland function can be applied, as described in [59]

$$\frac{P_n}{P_T} = G(\nu_1, \nu_2, j_1, j_2), \quad (28)$$

where

$$G(\nu_1, \nu_2, j_1, j_2) = \frac{2\nu_1 j_2}{B + \sqrt{B^2 - 4(\nu_2 - \nu_1)\nu_1 j_2}}, \quad (29)$$

$$B = \nu_2 - \nu_1 + j_1 \nu_2 + j_2 \nu_1. \quad (30)$$

In this formulation, P_n and P_T are the inactive and total PIN2 concentrations respectively. ν_1 and ν_2 are related to dephosphorylation and phosphorylation rates respectively. j_1 and j_2 are related to Michaelis-Menten constants for dephosphorylation and phosphorylation, respectively. In the calculation, ν_2 (labelled as ν_2^P) is taken directly proportional to the activated CPK29 concentration, K_{ac} shown as

$$\nu_2^P = 8E11 \times K_{ac}. \quad (31)$$

Subtracting ν_2^P from 1 and multiplying it with the total PIN2 concentration given in Table II, one can find the activated PIN2 concentration, P_a . The values for ν_1^P , j_1^P and j_2^P are given in Table III.

F. PIN2 and auxin

In [46], a very detailed mathematical model representing PIN and auxin distributions is presented which is also used in this block. For the purposes of this article, a grid of 11x11 cells is established as shown in Fig. 10. The parameter α_a , which describes the auxin biosynthesis rate, is doubled for the middle cells to represent auxin transport from the xylem. The left side of these cells is assumed to be hearing the voice and responding to it, while the other cells do not show any reaction. Response to the sound is modeled for the left-sided cells by a modification in their parameter δ_p , which describes PIN2 membrane dissociation rate, as follows

$$\delta_p^{modified} = \delta_p \times \frac{P_a(t_f)}{P_a(t_i)}, \quad (32)$$

where t_i and t_f are the starting and ending times of the simulation.

G. FER-ROPGEF-ROP6

The FERONIA protein activation by apoplasmic auxin can be modeled using the Hill equation, i.e.,

$$R_F = \frac{A^2}{k_F + A^2}, \quad (33)$$

where R_F represents the fraction of activated FERONIA proteins, and A represents the average auxin distribution in apoplast, averaging all four A_{ij} levels described in [46]. Multiplying this ratio with the total FERONIA concentration, which is given in Table II, will yield the

TABLE I
Parameters Extracted from Literature

Description	Symbol	Value	Unit
Bulk Density	ρ	1.30	gm/cm ³
Viscosity	η	1019	Pas
Shear Modulus	G	2.4	MPa
Auxin degradation rate	μ_a	0.5	min ⁻¹
auxin-TIR1 dissociation rate	γ_a	5	min ⁻¹
auxin-TIR1 binding rate	β_a	0.5	$\mu M^{-1} min^{-1}$
Maximum mRNA transcription rate	α_m	0.5	$\mu M min^{-1}$
Ratio of ARF-dependent to ARF ₂ - and double ARF-dependent mRNA transcription rates	ϕ_m	0.1	-
ARF-DNA binding threshold	θ_f	1	μM
ARF ₂ binding threshold	θ_w	10	μM
ARF + Aux/IAA-DNA binding threshold	θ_g	1	μM
Double ARF-DNA binding threshold	ψ_f	0.1	μM^2
ARF-Aux/IAA-DNA binding threshold	ψ_g	0.1	μM^2
Aux/IAA translation rate	α_r	5	min ⁻¹
Aux/IAA-auxin-TIR1 binding rate	β_r	5	$\mu M^{-1} min^{-1}$
Aux/IAA-auxin-TIR1 dissociation rate	γ_r	5	min ⁻¹
ARF-Aux/IAA binding rate	β_g	0.5	$\mu M^{-1} min^{-1}$
ARF-Aux/IAA dissociation rate	γ_g	5	min ⁻¹
PIN2 translation rate	α_p	5	min ⁻¹
PIN2-auxin-TIR1 binding rate	β_p	100	$\mu M^{-1} min^{-1}$
PIN-auxin-TIR1 dissociation rate	γ_p	5	min ⁻¹
PIN decay rate	μ_p	5	min ⁻¹
ARF dimerisation rate	β_f	0.5	$\mu M^{-1} min^{-1}$
ARF ₂ splitting rate	γ_f	5	min ⁻¹
Aux/IAA decay rate	μ_r	5	min ⁻¹
Auxin biosynthesis rate	α_a	0.5	$\mu M min^{-1}$
AUX1 biosynthesis rate	α_u	5	$\mu M min^{-1}$
AUX1 degradation rate	μ_u	5	min ⁻¹
Rate of AUX1 localisation to membrane	ω_u	0.5	$\mu m min^{-1}$
Rate of AUX1 dissociation from membrane	δ_u	0.05	min ⁻¹
Maximum rate of PIN2 localisation to membrane	ω_p	0.5	$\mu m min^{-1}$
Rate of PIN2 dissociation from membrane	δ_p	0.05	min ⁻¹
Fraction of protonated auxin in cell	κ_a^{ef}	0.004	-
Fraction of protonated auxin in wall	κ_a^{in}	0.24	-
Effective PIN2-induced auxin efflux	κ_p^{ef}	4.67	-
Effective AUX1-induced auxin influx	κ_u^{in}	3.56	-
Auxin membrane permeability	ϕ_a	0.55	$\mu m min^{-1}$
PIN2-induced auxin membrane permeability	ϕ_p	0.27	$\mu m \mu M^{-1} min^{-1}$
AUX1-induced auxin membrane permeability	$\tilde{\phi}_u$	0.55	$\mu m \mu M^{-1} min^{-1}$
Rate of auxin diffusion in apoplast	ϕ_A	67	$\mu m min^{-1}$
Sensitivity of PIN2 localisation to auxin flux	h	50	-
Auxin flux threshold	θ	2	-

active FERONIA concentration, F_a . FERONIA protein is thought to play a role in the phosphorylation of ROPGEF, although this may be an indirect effect [60]. Still, the previous phosphorylation model used for PIN2 phosphorylation by CPK29 (28) is also applied to ROPGEF activation by

TABLE II
Calculated/Assigned Values for the Model

Parameter	Value
A_M	91106.18695 \AA^2
Δx_d	7E-9 m
V_h	238.15 mV
σ_h	72.32 mmHg
ΔE	150E-3 V
Total RBOHC concentration	1.420265781E-8 mol/L
Total CPK29 concentration	1.724252492E-7 mol/L
Total FERONIA concentration	4.370431894E-7 mol/L
Total PIN2 concentration	3.518272425E-8 mol/L
Total ROPGEF4 concentration	4.634551495E-9 mol/L
Total ROP6 concentration	5.830564784E-8 mol/L
F	96485 C/mol
R	8.314 J/molK
T	298 K
V	1E - 5 L
G_a	17E-12 S
l	15.6871

the FERONIA protein. In this case, ν_2 is taken directly proportional to the activated FERONIA concentration, F_a shown as

$$\nu_2^R = 8E11 \times F_a. \quad (34)$$

The values for ν_1^R , j_1^R and j_2^R are given in Table III. Applying a similar logic and utilizing the total ROPGEF concentration given in Table II, the activated ROPGEF concentration, G_a , is found. In this calculation, ROPGEF4 concentration is used specifically. Then, the Michaelis-Menten equation is used once more to model the ROP6 activation by ROPGEF as follows

$$v_O = \frac{v_{Pm} G_a(t)}{k_P + G_a(t)}, \quad (35)$$

where integration of v_O over time yields the active ROP6 concentration. Then, the variable ω_p which is related to the maximum rate of PIN2 localisation to membrane is modified for each cell as follows

$$\omega_p^{modified} = \delta_p \times \frac{O_a(t_f)}{O_a(t_i)}, \quad (36)$$

where O_a represents the activated ROP6 concentration, as ROP6 activity is proposed to inhibit internalization of PIN2 through stabilization of actin filaments in roots [48].

VI. Simulation Results

In this section, the cell wall and MCA2 channel blocks are inspected in detail. Moreover, some critical results of the simulation are provided. Some specific parameters and their values are given in Table II, and fixed chosen parameter values of the model are shown in Table III.

Simulations were performed for 150 seconds in MATLAB R2023b. Two different time steps were employed: 0.0005 s (2 kHz sample rate) for real-time flow modeling (sound propagation and MCA2 response), and 0.5 s for internal cell processes. The 0.5 s step is based on the assumption that the MCA2 channels produce two responses per second.

TABLE III
Chosen Values for Model Parameters

k_F	1E-6 mol/L	N_1	100	x_m	1m
μ_s	0.01 Pa sec	μ_w	13E10 Pa sec	τ_w	0.02 sec
τ_s	0.001 sec	Y	0.5 Pa	k_V	32.64 mV
k_σ	16.13 mmHg	$c_c(t_i)$	150 nM	k_d	$0.01 Pa^{-1}$
A_C	$1.9635E-17 m^2$	n_C	40	k_C	$1e-7 M$
v_{Hm}	$4E-5 molL^{-1}sec^{-1}$	m_H	$1E-9 mol/L$	v_{sm}	$1E-5 molL^{-1}sec^{-1}$
m_s	$1E-4 mol/L$	n_a	40	k_a	$1.336E-8 mol/L$
z	2	k_{eff1}	0.3	k_{eff2}	0.16
k_K	$1E-23 mol/L$	ν_1^P	$5 molL^{-1}sec^{-1}$	j_1^P	0.1 mol/L
j_2^P	5 mol/L	ν_1^R	$5 molL^{-1}sec^{-1}$	j_1^R	0.1 mol/L
j_2^R	5 mol/L	v_{Pm}	$0.1 molL^{-1}sec^{-1}$	k_P	0.05 mol/L

The cell wall takes stress (Pa) on the cell walls as its input and yields pressure (Pa) on one MCA2 channel. To understand the frequency characteristics of this block, a spectrogram of the input and output of the system is obtained as shown in Fig. 4. It is observed that the cell wall enhances the frequency components in the 0-1000 Hz range. Moreover, from Fig. 5 one observes that the cell wall preserves much of the input timing and shape in the operating frequency since there is a high correlation with small time lags.

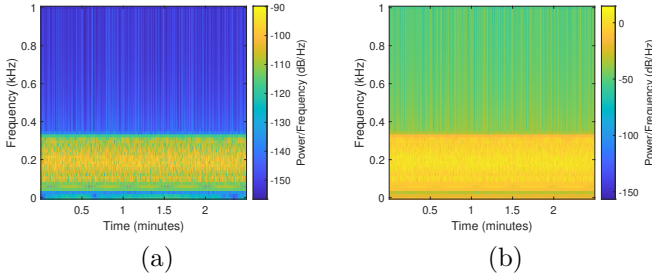


Fig. 4. Spectrograms of (a) input and (b) output signals of the cell wall.

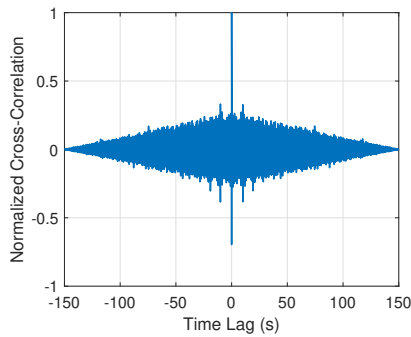


Fig. 5. Cross-Correlation of input and output signals of the Cell Wall.

The MCA2 Channels block takes the pressure (*mmHg*) on an MCA2 channel as its input and produces the total Ca^{2+} influx concentration (*nM*) through the MCA2

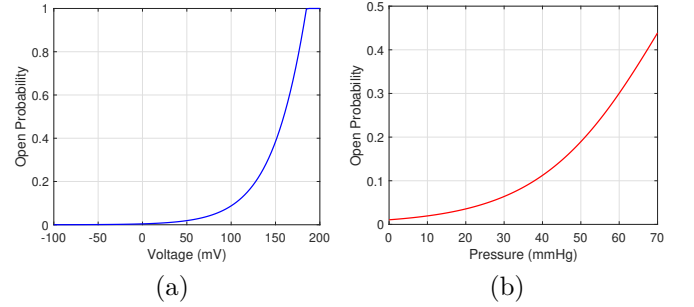


Fig. 6. Open state probability characteristics of the MCA2 channel: (a) variation with voltage at a pressure level of 65 *mmHg*, and (b) variation with pressure at 150 *mV*.

channels. The lowpass filter in Fig. 3 is a Butterworth filter with a cut-off frequency of 250 *Hz*. The open probability of an MCA2 channel is plotted in Fig. 6. Mathematically, after the filtering operation, the signal is downsampled to biological time steps. Moreover, the output of the MCA2 channel is characterized as a discrete-time signal. To understand the behavior of the MCA2 Channels block, different inputs are applied. Response to a shifted impulse is observed to result in only one spike, and the step response is observed to be another step function. The output to a sinusoidal input exhibits periodic oscillations with a rectified shape. Furthermore, a possible input-output signal pair is also calculated. These results can be observed in Fig. 7. As it can be seen in Fig. 7(d)–(h), characteristics of Ca^{2+} influx through MCA2 channels are very similar to the current spikes given in [41].

In Fig. 8, the change in cytosolic calcium concentration is illustrated. Upon sound stimulation, a rapid increase in cytosolic Ca^{2+} levels is observed, facilitated by the Ca^{2+} - ROS Hub. Subsequently, the concentration stabilizes within the range of 220–240 *nM*. These results are consistent with the findings reported in [16].

Fig. 9 shows the change of apoplasmic H_2O_2 levels with time. The shape of this signal is very similar to the cytosolic Ca^{2+} concentration, since it also increases for

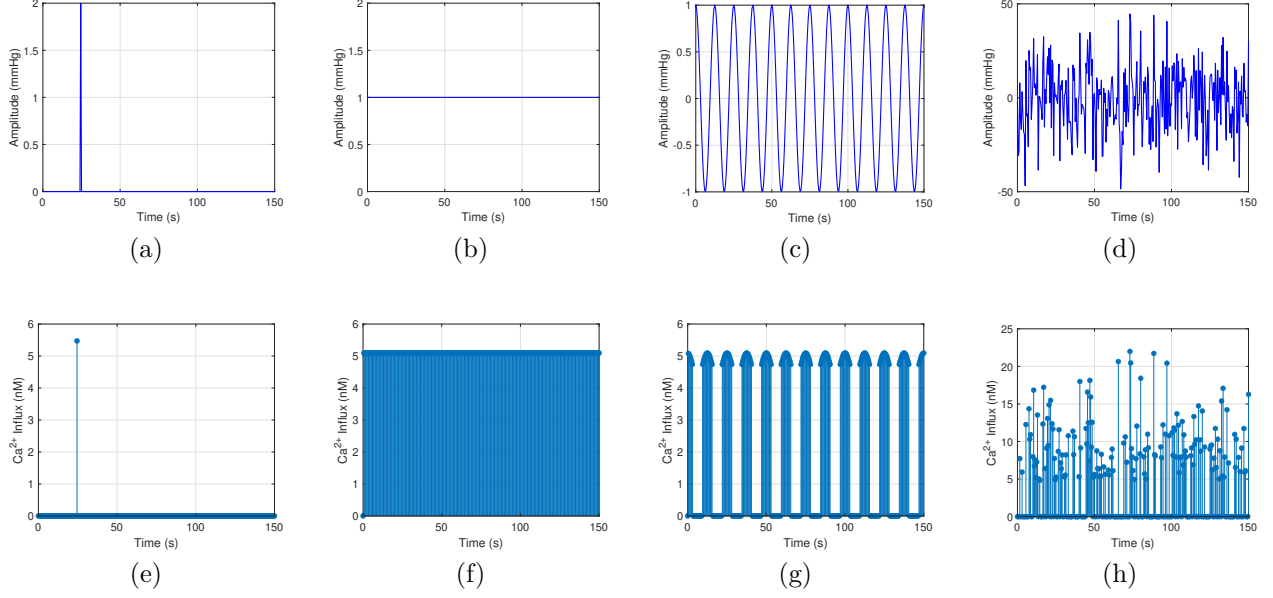


Fig. 7. MCA2 channel responses to various input signals: (a) impulse input and (e) its output; (b) step input and (f) its output; (c) cosine input with frequency 0.08 Hz and (g) its output; (d) a possible input and (h) its output.

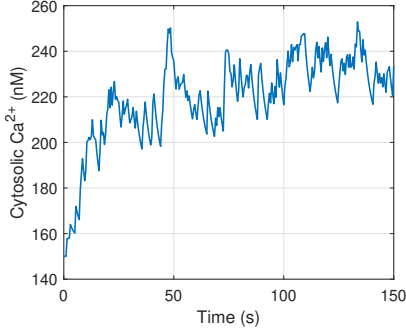


Fig. 8. Change of cytosolic Ca^{2+} concentration under sound stimuli through time.

some time and reaches a steady interval.

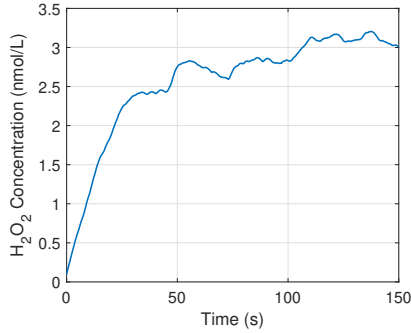


Fig. 9. Change of apoplastic H_2O_2 concentration under sound stimuli through time.

Fig. 10 shows an example 11x11 root cell grid where the middle column is assumed to be xylem where auxin flows from shoots to roots. Left-sided cells have modified δ_p parameters as explained in (32), representing the reaction to the sound stimuli. As can be seen, on the left side, the

sound stimuli stops the flow of auxin while on the right side, some kind of auxin distribution occurs. With gravity, auxin will mostly gather on the edges of the roots on the right side, and those parts will grow faster resulting in the bending of roots towards the water flow.

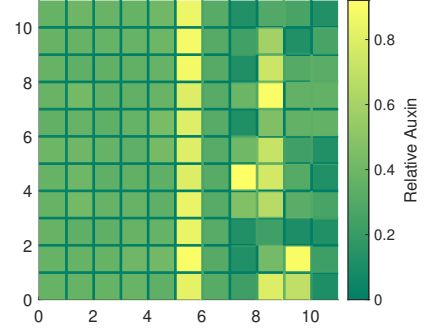


Fig. 10. Relative auxin levels of the 11x11 cell grid. Left side is assumed to be responding to sound stimuli while the right side is not.

VII. Communication-Theoretic Analysis of Plant Acoustic Sensing

In this section, our objective is to quantify how variations in the characteristics of incoming acoustic stimuli influence the physiological responses they elicit in plants. Specifically, we investigate how changes in the mean frequency and mean amplitude of the sound wave affect plants' ability to elicit a response. Moreover, we examine how long it takes after the stimulus for the plant to generate a clear physiological response. To formalize these questions within a communication-theoretic framework, we performed a bit-error rate (BER) analysis.

From a communication-theoretic standpoint, the system can be treated as a digital link. A logical "1" represents

the presence of water flow beneath the soil and triggers a sound wave generated by (5); a logical “0” represents its absence, so no acoustic signal is emitted. The receiver declares bit 1 when a strong polar auxin distribution is present in the roots and declares bit 0 when no such distribution is observed. Simulations show that a visible polar distribution appears whenever the Activated PIN2 Ratio (APR), defined as the ratio of activated PIN2 concentration at the end of a bit interval to that at its start exceeds 5. Thus the decision rule can be written as

$$\hat{b} = \begin{cases} 1, & \text{if } APR > 5 \\ 0, & \text{otherwise} \end{cases}. \quad (37)$$

In Fig. 11 an example input-output bit comparison is given. The corresponding cytosolic Ca^{2+} concentration plot is also provided in Fig. 12. Here for one bit of information, the signal is sent for 150 seconds, and 5 bits are sent in total.

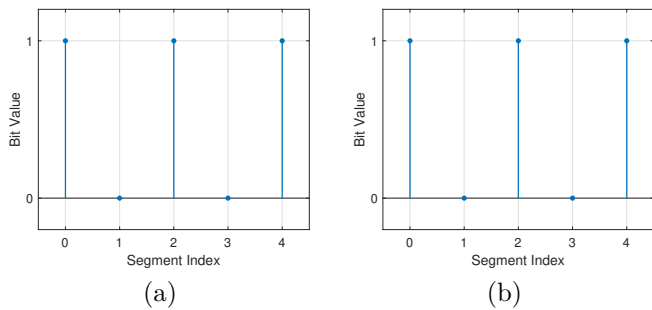


Fig. 11. (a) Transmitted and (b) received bits.

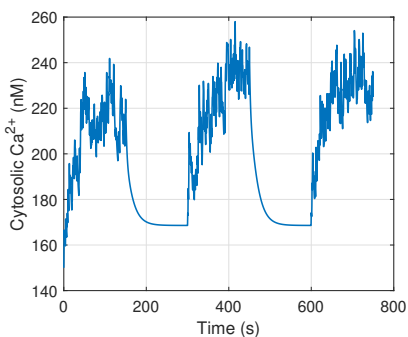
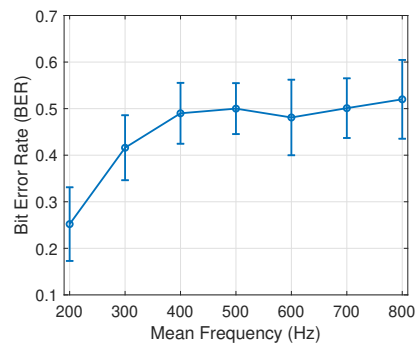
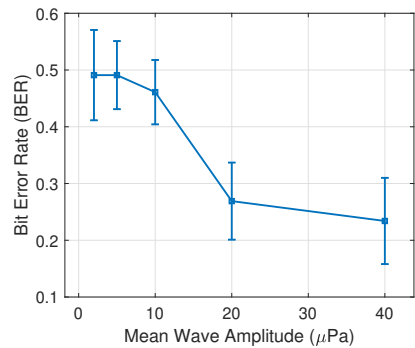


Fig. 12. Ca^{2+} concentration change due to sound waves.

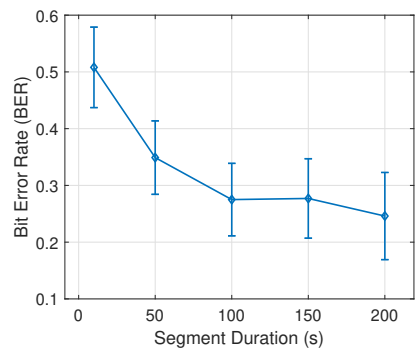
Using this concept, one can inspect the performance of the system with varying levels of sound frequency and amplitude. The performance of the system is evaluated as a function of the mean acoustic frequency. The mean of the Gaussian distributed carrier f_n is stepped through [200, 300, 400, 500, 600, 700, 800] Hz where all other parameters are kept as their original values. For each mean value, 20 independent runs are carried out, each transmitting 50 bits and the bit-error rate (BER) is calculated. The results, shown in Fig. 13(a), reveal a pronounced increase in BER as the mean frequency increases from 200 Hz.



(a)



(b)



(c)

Fig. 13. Bit Error Rate (BER) analysis under varying system parameters: (a) mean frequency, (b) mean amplitude, and (c) plant decision time.

To investigate the effect of the sound amplitude A_s on the system performance, the mean of the Gaussian distributed amplitude level is iterated over [2, 5, 1, 20, 40] μPa where all other parameters are kept as their original values. Similarly, for each mean value, 20 independent runs are performed, each transmitting 50 bits and the bit-error rate (BER) is calculated. Results are shown in Fig. 13(b). It is observed that for small pressure levels, the plant is insensitive to sound waves.

Plant decision time describes how much time is needed for the plant to correctly decide on the input bit. Previously this was set to 150 seconds. To understand how fast plants can decide correctly whether there is a water flow, plant decision time is varied across [10, 50, 100, 150, 200] where all other parameters are kept as their original values. For each value, 20 independent runs are performed,

each transmitting 50 bits and the bit-error rate (BER) is calculated. The resulting plot can be seen in Fig. 13(c). It becomes clear that the plant needs at least 100 seconds to decide whether there is water flow or not.

VIII. Conclusion

In this paper, a mathematical model describing how sound waves affect plants is proposed for the first time in the literature. Water flow under the soil is considered the source of the sound waves, the soil is the channel for the sound wave propagation, and the root cells are the receivers of the stimuli. How sound stimuli might trigger a response in plants is described by considering mechanosensitive channels, the Ca-ROS Hub proposal, and the role of auxin hormone in plants.

The analysis reveals that initially increased cytosolic calcium concentration can induce ROS production and create a positive feedback loop to increase cytosolic calcium concentration. Moreover, it is confirmed that PIN2 redistribution caused by sound stimuli may lead to the bending of roots.

Studying phytoacoustics requires an understanding of various aspects of plant biology, and there are many questions that need to be answered. More research is needed to address key areas, including:

- How do plants extract different meanings from different sound waves?
- What is the evolutionary background of sound perception in plants?
- Can plants transmit meaningful messages using sound waves?
- Can plants communicate with each other in this manner?
- Do plants have any form of acoustic memory? If so, can this be transferred to subsequent generations?
- How exactly can farmers make use of sound wave stimuli?

Exploring this field may open new perspectives on plant behavior and shed light on how we can utilize sound waves to enhance plant growth and health.

References

- [1] A. B. Kilic and O. B. Akan, "Information and Communication Theoretical Foundations of the Internet of Plants, Principles, Challenges, and Future Directions," September 2025.
- [2] J. A. Milburn and R. Johnson, "The conduction of sap - ii. detection of vibrations produced by sap cavitation in ricinus xylem," *Planta*, vol. 69, no. 1, p. 43 – 52, 1966.
- [3] M. Wei, C. ying Yang, and S. hua Wei, "Enhancement of the differentiation of protocorm-like bodies of dendrobium officinale to shoots by ultrasound treatment," *Journal of Plant Physiology*, vol. 169, no. 8, pp. 770–774, 2012.
- [4] R. Ghosh et al., "Exposure to sound vibrations lead to transcriptomic, proteomic and hormonal changes in arabidopsis," *Scientific Reports*, vol. 6, p. 33370, 09 2016.
- [5] M. Veits et al., "Flowers respond to pollinator sound within minutes by increasing nectar sugar concentration," *Ecology Letters*, vol. 22, 07 2019.
- [6] H. Zhao, J. Wu, B. Xi, and B. Wang, "Effects of sound-wave stimulation on the secondary structure of plasma membrane protein of tobacco cells," *Colloids and Surfaces B: Biointerfaces*, vol. 25, no. 1, pp. 29–32, 2002.
- [7] W. Bochu, C. Xin, W. Zhen, F. Qizhong, Z. Hao, and R. Liang, "Biological effect of sound field stimulation on paddy rice seeds," *Colloids and Surfaces B: Biointerfaces*, vol. 32, no. 1, pp. 29–34, 2003.
- [8] A. Z. Babar and O. B. Akan, "Sustainable and Precision Agriculture with the Internet of Everything (IoE)," January 2025.
- [9] B. Maitra, M. Gulgun, E. Bardakci, O. Cetinkaya, and O. B. Akan, "Internet of harvester nano things: A future prospects," 2023.
- [10] I. Khait et al., "Sounds emitted by plants under stress are airborne and informative," *Cell*, vol. 186, no. 7, pp. 1328–1336.e10, 2023. [Online]. Available: <https://www.sciencedirect.com/science/article/pii/S0092867423002623>
- [11] M.-J. Jeong et al., "Plant gene responses to frequency-specific sound signals," *Mol Breeding*, vol. 21, pp. 217–226, 02 2008.
- [12] I. López-Ribera and C. Vicient, "Drought tolerance induced by sound in arabidopsis plants," *Plant Signaling & Behavior*, vol. 12, pp. 00–00, 08 2017.
- [13] R. Hedrich, "Ion channels in plants," *Physiological Reviews*, vol. 92, no. 4, pp. 1777–1811, 2012, PMID: 23073631.
- [14] T. A. G. Initiative, "Analysis of the genome sequence of the flowering plant arabidopsis thaliana," *Nature*, vol. 408, no. 6814, pp. 796–815, 2000.
- [15] F. Merdan, "Created in biorender," <https://BioRender.com/46tpf6c>, 2025, bioRender Illustration.
- [16] A. Rodrigo-Moreno et al., "Root phonotropism: Early signalling events following sound perception in arabidopsis roots," *Plant Science*, vol. 264, pp. 9–15, 2017.
- [17] J. Liu, Y. Niu, J. Zhang, Y. Zhou, Z. Ma, and X. Huang, "Ca²⁺ channels and ca²⁺ signals involved in abiotic stress responses in plant cells: recent advances," *Plant Cell, Tissue and Organ Culture (PCTOC)*, vol. 132, no. 3, pp. 413–424, 2018.
- [18] V. Demidchik and S. Shabala, "Mechanisms of cytosolic calcium elevation in plants: the role of ion channels, calcium extrusion systems and nadph oxidase-mediated 'ros-ca²⁺ hub'," *Functional plant biology : FPB*, vol. 45, no. 2, p. 9–27, January 2018.
- [19] E. Krol and K. Trebacz, "Ways of ion channel gating in plant cells," *Annals of Botany*, vol. 86, no. 3, pp. 449–469, 2000.
- [20] A. Tyagi, S. Ali, S. Park, and H. Bae, "Deciphering the role of mechanosensitive channels in plant root biology: perception, signaling, and adaptive responses," *Planta*, vol. 258, no. 6, p. 105, 2023.
- [21] M. Nakano, K. Iida, H. Nyunoya, and H. Iida, "Determination of Structural Regions Important for Ca²⁺ Uptake Activity in Arabidopsis MCA1 and MCA2 Expressed in Yeast," *Plant and Cell Physiology*, vol. 52, no. 11, pp. 1915–1930, 09 2011.
- [22] S. Kamano et al., "Transmembrane topologies of ca²⁺-permeable mechanosensitive channels mca1 and mca2 in arabidopsis thaliana," *Journal of Biological Chemistry*, vol. 290, no. 52, pp. 30901–30909, 2015.
- [23] K. Nishii, M. Möller, and H. Iida, "Mix and match: Patchwork domain evolution of the land plant-specific ca²⁺-permeable mechanosensitive channel mca," *PLOS ONE*, vol. 16, no. 4, pp. 1–20, 04 2021.
- [24] T. Yamanaka et al., "MCA1 and MCA2 That Mediate Ca²⁺ Uptake Have Distinct and Overlapping Roles in Arabidopsis," *Plant Physiology*, vol. 152, no. 3, pp. 1284–1296, 01 2010.
- [25] H. Semerádova, J. C. Montesinos, and E. Benkova, "All roads lead to auxin: Post-translational regulation of auxin transport by multiple hormonal pathways," *Plant Communications*, vol. 1, no. 3, p. 100048, 2020, focus Issue on Plant Hormones (Organizing Editors: Steven Smith, Jan Hejálto, Yonghong Wang, Daixin Xie).
- [26] M. Du, E. P. Spalding, and W. M. Gray, "Rapid auxin-mediated cell expansion," *Annual Review of Plant Biology*, vol. 71, pp. 379–402, 2020, epub 2020 Mar 4.
- [27] E. Barbez, K. Dünser, A. Gaidora, T. Lendl, and W. Busch, "Auxin steers root cell expansion via apoplastic ph regulation in arabidopsis thaliana," *Proceedings of the National Academy of Sciences*, vol. 114, no. 24, pp. E4884–E4893, 2017.
- [28] D. Dietrich, "Hydrotropism: how roots search for water," *Journal of Experimental Botany*, vol. 69, no. 11, pp. 2759–2771, 02 2018.

- [29] Y. Wexler, J. I. Schroeder, and D. Shkolnik, "Hydrotropism mechanisms and their interplay with gravitropism," *The Plant Journal*, vol. 118, no. 6, pp. 1732–1746, 2024.
- [30] M. A. Biot, "Theory of Propagation of Elastic Waves in a Fluid-Saturated Porous Solid. I. Low-Frequency Range," *The Journal of the Acoustical Society of America*, vol. 28, no. 2, pp. 168–178, 03 1956.
- [31] —, "Theory of Propagation of Elastic Waves in a Fluid-Saturated Porous Solid. II. Higher Frequency Range," *The Journal of the Acoustical Society of America*, vol. 28, no. 2, pp. 179–191, 03 1956.
- [32] M. A. Al Mosh, M. Hardie, T. Choudhury, and J. Kamruzzaman, "Wireless underground sensor communication using acoustic technology," *Sensors*, vol. 24, no. 10, 2024.
- [33] S. L. Kramer, *Geotechnical Earthquake Engineering*. New Delhi, India: Pearson Education, 1996.
- [34] M. Gagliano, S. Mancuso, and D. Robert, "Towards understanding plant bioacoustics," *Trends in Plant Science*, vol. 17, no. 6, pp. 323–325, 2012.
- [35] M. Gagliano, M. Grimonprez, M. Depczynski, and M. Renton, "Tuned in: plant roots use sound to locate water," *Oecologia*, vol. 184, pp. 151–160, 05 2017.
- [36] S. Liu, J. Jiao, T. J. Lu, F. Xu, B. G. Pickard, and G. M. Genin, "Arabidopsis leaf trichomes as acoustic antennae," *Biophysical Journal*, vol. 113, no. 9, pp. 2068–2076, 2017.
- [37] X. Peng et al., "Acoustic radiation force on a long cylinder, and potential sound transduction by tomato trichomes," *Biophysical Journal*, vol. 121, no. 20, pp. 3917–3926, 2022.
- [38] L. H. Zhou et al., "The arabidopsis trichome is an active mechanosensory switch," *Plant, cell & environment*, vol. 40, 02 2016.
- [39] A. Fruleux, S. Verger, and A. Boudaoud, "Feeling stressed or strained? a biophysical model for cell wall mechanosensing in plants," *Frontiers in Plant Science*, vol. 10, 2019. [Online]. Available: <https://www.frontiersin.org/journals/plant-science/articles/10.3389/fpls.2019.00757>
- [40] H. Shigematsu, K. Iida, M. Nakano, P. Chaudhuri, H. Iida, and K. Nagayama, "Structural characterization of the mechanosensitive channel candidate mca2 from arabidopsis thaliana," *PLoS one*, vol. 9, p. e87724, 01 2014. [Online]. Available: <https://doi.org/10.1371/journal.pone.0087724>
- [41] K. Yoshimura, K. Iida, and H. Iida, "Mcas in arabidopsis are ca2+-permeable mechanosensitive channels inherently sensitive to membrane tension," *Nature communications*, vol. 12, no. 1, 2021. [Online]. Available: <https://doi.org/10.1038/s41467-021-26363-z>
- [42] A. Lewit-Bentley and S. Réty, "Ef-hand calcium-binding proteins," *Current Opinion in Structural Biology*, vol. 10, no. 6, pp. 637–643, 2000.
- [43] I. Pottosin and I. Zepeda-Jazo, "Powering the plasma membrane Ca2+-ROS self-amplifying loop," *Journal of Experimental Botany*, vol. 69, no. 14, pp. 3317–3320, 06 2018.
- [44] V. Demidchik, S. Shabala, S. Isayenkov, T. A. Cuin, and I. Pottosin, "Calcium transport across plant membranes: mechanisms and functions," *New Phytologist*, vol. 220, no. 1, pp. 49–69, 2018.
- [45] H. Lee, A. Ganguly, S. Baik, and H.-T. Cho, "Calcium-dependent protein kinase 29 modulates PIN-FORMED polarity and Arabidopsis development via its own phosphorylation code," *The Plant Cell*, vol. 33, no. 11, pp. 3513–3531, 08 2021.
- [46] H. R. Allen and M. Ptashnyk, "Mathematical modelling of auxin transport in plant tissues: Flux meets signalling and growth," *Bulletin of Mathematical Biology*, vol. 82, no. 2, p. 17, 2020.
- [47] C. Li, H.-M. Wu, and A. Y. Cheung, "FERONIA and Her Pals: Functions and Mechanisms," *Plant Physiology*, vol. 171, no. 4, pp. 2379–2392, 06 2016.
- [48] D. Lin et al., "A rop gtpase-dependent auxin signaling pathway regulates the subcellular distribution of pin2 in arabidopsis roots," *Current Biology*, vol. 22, no. 14, pp. 1319–1325, 2012.
- [49] X. Han, Y. Shi, G. Liu, Y. Guo, and Y. Yang, "Activation of rop6 gtpase by phosphatidylglycerol in arabidopsis," *Frontiers in Plant Science*, vol. 9, 2018. [Online]. Available: <https://www.frontiersin.org/journals/plant-science/articles/10.3389/fpls.2018.00347>
- [50] B. Hille, *Ion Channels of Excitable Membranes*, 3rd ed. Sunderland, Mass.: Sinauer Associates, 2001.
- [51] M. Ben-Johny et al., "Towards a unified theory of calmodulin regulation (calmodulation) of voltage-gated calcium and sodium channels," *Current Molecular Pharmacology*, vol. 8, no. 2, pp. 188–205, 2015.
- [52] T. V. Martins, M. J. Evans, H. C. Woolfenden, and R. J. Morris, "Towards the physics of calcium signalling in plants," *Plants (Basel)*, vol. 2, no. 4, pp. 541–588, September 27 2013. [Online]. Available: <https://www.ncbi.nlm.nih.gov/pmc/articles/PMC4844391/>
- [53] S. Gilroy et al., "ROS, Calcium, and Electric Signals: Key Mediators of Rapid Systemic Signaling in Plants," *Plant Physiology*, vol. 171, no. 3, pp. 1606–1615, 05 2016.
- [54] K. Park, J. Knoblauch, K. Oparka, and K. Jensen, "Controlling intercellular flow through mechanosensitive plasmodesmata nanopores," *Nature Communications*, vol. 10, 08 2019.
- [55] w.-G. Choi, G. Miller, I. Wallace, J. Harper, R. Mittler, and S. Gilroy, "Orchestrating rapid long-distance signaling in plants with ca2+, ros, and electrical signals," *The Plant Journal*, vol. 90, 01 2017.
- [56] F. Resentini, C. Ruberti, M. Grenzi, M. C. Bonza, and A. Costa, "The signatures of organellar calcium," *Plant Physiology*, vol. 187, no. 4, pp. 1985–2004, 04 2021.
- [57] B. Dubreuil, O. Matalon, and E. D. Levy, "Protein abundance biases the amino acid composition of disordered regions to minimize non-functional interactions," *Journal of Molecular Biology*, vol. 431, no. 24, pp. 4978–4992, 2019.
- [58] N. Puneekar, *Enzymes: Catalysis, Kinetics and Mechanisms*, 1st ed. Springer Singapore, 2018.
- [59] J. J. Tyson, K. C. Chen, and B. Novak, "Sniffers, buzzers, toggles and blinkers: dynamics of regulatory and signaling pathways in the cell," *Current Opinion in Cell Biology*, vol. 15, no. 2, pp. 221–231, 2003.
- [60] S. A. Kessler, H. Lindner, D. S. Jones, and U. Grossniklaus, "Functional analysis of related crkl1 receptor-like kinases in pollen tube reception," *EMBO reports*, vol. 16, no. 1, pp. 107–115, 2015.



Fatih Merdan completed his high school education at Kırıkkale Science High School. He received his B.Sc. degree in Electrical and Electronics Engineering from Middle East Technical University. He is currently pursuing his M.Sc. degree in Electrical and Electronics Engineering under the supervision of Prof. Akan at Koç University, Istanbul, Turkey.



Ozgur B. Akan (Fellow, IEEE) received the PhD from the School of Electrical and Computer Engineering Georgia Institute of Technology Atlanta, in 2004. He is currently the Head of Internet of Everything (IoE) Group, with the Department of Engineering, University of Cambridge, UK and the Director of Centre for neXt-generation Communications (CXC), Koç University, Turkey. His research interests include wireless, nano, and molecular communications and Internet of Everything.